Wiley: Zeng, J., Qiu, N., Zhang, J., Wang, X., Redshaw, C., Feng, X., Lam, J. W. Y., Zhao, Z., Tang, B. Z., Y-Shaped Pyrene-Based Aggregation-Induced Emission Blue Emitters for High-Performance OLED Devices. *Adv. Optical Mater.* 2022, 2200917, which has been published in final form at https://doi.org/10.1002/adom.202200917. This article may be used for non-commercial purposes in accordance with Wiley Terms and Conditions for self-archiving.

Y-shaped pyrene-based aggregation-induced emission blue emitters for high-performance OLED devices

Jin Zeng, Nuoling Qiu, Jianyu Zhang, Xiaohui Wang, Carl Redshaw, Xing Feng, Jacky W. Y. Lam, Zujin Zhao,* and Ben Zhong Tang,**

J. Zeng, X. Wang, Dr. X. Feng
Guangdong Provincial Key Laboratory of Information Photonics Technology
School of Material and Energy, Guangdong University of Technology
Guangzhou 510006, P. R. China.
Email: hyxhn@sina.com (X. Feng)

N. Qiu, Prof. Z. Zhao, Prof. B. Z. Tang
State Key Laboratory of Luminescent Materials and Devices
Guangdong Provincial Key Laboratory of Luminescence from Molecular Aggregates
South China University of Technology, Guangzhou, 510640, P. R. China.
E-mail: mszjzhao@scut.edu.cn (Z. Zhao)

J. Zhang, Prof. J. W. Y. Lam, Prof. B. Z. Tang
Department of Chemistry, the Hong Kong Branch of Chinese National Engineering Research Center for Tissue Restoration and Reconstruction, and Guangdong-Hong Kong-Macro Joint Laboratory of Optoelectronic and Magnetic Functional Materials, The Hong Kong University of Science and Technology, Clear Water Bay, Kowloon, Hong Kong, China

Prof. C. Redshaw
Department of Chemistry, University of Hull,
Cottingham Road, Hull, Yorkshire HU6 7RX UK.

Dr. X. Feng

Guangdong Provincial Key Laboratory of Luminescence from Molecular Aggregates (South China University of Technology),
Guangzhou 510640, P. R. China.

Prof. B. Z. Tang
School of Science and Engineering, Shenzhen Institute of Aggregate Science and Technology, The Chinese University of Hong Kong, Shenzhen, Guangdong 518172, China. E-mail: tangbenz@cuhk.edu.cn

Keywords: pyrene, aggregation-induced emission, blue emitter, organic light-emitting diode, hot exciton mechanism

Abstract: The proposed concept of aggregation-induced emission (AIE) has offered an efficient strategy to design high-performance luminescent materials. Herein, three blue emitters containing a pyrene core decorated with either triphenylamine or tetraphenylethylene units are presented. The designed compounds **Py-TPA** and **Py-2TPE** are AIE-active materials with blue emission from 464 to 478 nm in the solid state, whereas **Py-2TPA** is not. Moreover, the enhanced thermal stability of compounds **Py-TPA** and **Py-2TPE** allows for their utilization as emitter layers for the fabrication of blue organic light-emitting diode (OLED) devices. The devices exhibited excellent electroluminescence emission with maximum $\lambda_{max\ em}$ in the range 456-482 nm with a maximum external quantum efficiency of 7.27%, high exciton utilization efficiency (77.3%), and low turn-on voltage (≤ 3.1 V), as well as low-efficiency roll-off. Theoretical calculations revealed that the high exciton utilization efficiency (η_r) originates from the triplet excitons at T_2 to the lowest single excited (S_1) state *via* a reverse intersystem crossing (RISC) process following the principle of the "hot exciton" mechanism. This article not only provides powerful evidence revealing the advantages of pyrene-based AIEgens for OLED applications, but also offers a new approach for designing pyrene-based "hot exciton" materials for next-generation OLEDs.

1. Introduction

Since Tang and VanSlyke developed the first organic light-emitting diode (OLED) device in 1987,[1] OLED devices as commercial products have crept into our lives and have attracted industrial and academic interest. Indeed, they are now considered as central to the next generation flat-panel displays and solid-state lighting technologies.[2] High-efficiency organic

luminescent materials are one of the most important components for constructing OLEDs, due to their outstanding advantages, such as low-cost, precise molecular structures, easy preparation, and purification. Up to now, many types of organic fluorophores, such as fluorescent/phosphorescent materials,[3] organic thermally activated delayed fluorescent (TADF) materials,[4] and radicals,[5], have been utilized as the emissive layer for OLED applications. In the case of OLED lighting, 25% of the excitons are generated in the singlet state and 75% of the excitons in the triplet state by spin statistics.[6-8] Theoretically, TADF materials can realize 100% exciton utilization efficiency (η_r) via triplet-singlet conversion. In comparison, the value of η_r is 75% for phosphorescent materials and only 25% for fluorescent materials. However, the serious efficiency roll-off of OLEDs based on TADF/phosphorescent materials can be observed by triplet-involved annihilation.[9] Thus, how to maximize the η_r and simultaneously decrease the efficiency roll-off are key points for exploiting high-performance OLEDs.

Generally, TADF molecules can harvest the triplet excitons from the lowest triplet (T_1) to the lowest singlet excited (S_1) state by a reverse intersystem crossing (RISC) process. Recently, Ma *et al*. proposed the "hot exciton mechanism" to improve the η_r value to the theoretical value up to 100%,[10] *via* upper triplet levels (T_n, n>1).[11] In contrast to the traditional TADF mechanism, the hot exciton mechanism involves fast RISC from the high-lying triplet state (T_n, n>1) to the excited singlet state (S_m, $m \geqslant 1$). Besides, this process can weaken the exciton annihilation and improve the η_r value of OLED devices.[12]

Pyrene and its derivatives are important members of the polycyclic aromatic hydrocarbons, which have been widely explored in OLEDs, fluorescent probes, etc., due to their excellent fluorescence properties with high quantum yields, high thermal stability, and good charge carrier mobility.[13] However, the planar fused-ring geometric structure of pyrene prefers to form a dimer by intermolecular interactions (such as π-π stacking, C-H···π, as well as several hydrogen bonds), which may lead to a fluorescence quenching, defined as the aggregation-caused quenching (ACQ) effect.[14, 15] Much effort has been devoted to constructing high-performance pyrene-based fluorophores by molecular tailoring strategies *via* inhibiting the π-π stacking in the solid state, to realize the high efficiency of the solid-state emission of organic luminescent materials.[16, 17] The concept of aggregation-induced emission (AIE) was coined by Tang *et al*. in 2001,[18] and the restriction of intramolecular motion (RIM) mechanism was proposed to elucidate the AIE phenomenon, as well as guide the design of organic molecules with AIE characteristics for various applications.[19, 20] Inspired by the excellent photophysical properties of AIE luminogens (AIEgens), the construction of pyrene-based AIEgens is also

regarded as an ideal strategy to solve the ACQ effect of pyrene and its derivatives. Li *et al*. reported a 2,7-substituted pyrene (Py-2TP) with AIE characteristics, demonstrating intensive blue light emission with high external quantum efficiencies up to 3.46% in non-doped OLEDs.[21] Moreover, our group has conducted systematic comparative studies of the advantages of pyrene AIEgens for OLED applications *versus* traditional pyrene-based emitters. For example, fluorescent OLED devices based on pyrene AIEgens exhibit good electroluminescence (EL) performance with brightness, low turn-on voltage, and low-efficiency roll-off [22]. Following the hot exciton mechanism, Lu and coworkers presented a highly efficient and blue-emitting material 9-phenyl-10-(4-(pyren-1-yl)phenyl)-9H-pyreno[4,5-d]imidazole (PyPI-Py) with a maximum brightness (L_{max}), maximum current efficiency ($\eta_{c\ max}$) and maximum external quantum efficiency ($\eta_{ext\ max}$) of 75,687 cd m^{-2}, 13.38 cd A^{-1}, and 8.52%, respectively.[23] Thus, inspired by the "hot exciton mechanism" and the advantages of pyrene-based AIEgens in OLEDs, we attempted to design and synthesize pyrene-based AIEgens containing a pyrene core decorated with either triphenylamine (TPA) or tetraphenylethylene (TPE) units for high-performance blue OLED devices. The molecules display pure blue/sky blue emission with AIE characteristics. Moreover, the selected pyrene-based AIEgens **Py-TPA** and **Py-2TPE** were utilized as the emitting layer for OLEDs with excellent electroluminescence properties and high η_r value (up to 7.27%) and a low turn-on voltage (less than 3.1 V).

2. Synthesis and characterization

The molecular structures of three pyrene-based compounds **Py-TPA**, **Py-2TPA** and **Py-2TPE** are presented in Figure 1. The intermediates 1-bromo-7-*tert*-butyl pyrene and 1,3-dibromo-7-*tert*-butyl pyrene were synthesized according to a previous report.[24] The target compounds were successfully synthesized *via* a conventional Suzuki-Miyaura coupling reaction between the pyrene-based intermediates and the corresponding arylboronic acids in high yield. The molecular structures were further characterized by $^{1}H/^{13}C$ NMR spectroscopy and high-resolution mass spectrometry (HRMS). Due to the presence of bulky groups of the TPA or TPE groups and the twisted structure, together with the *tert*-butyl group at the 7-position of pyrene, the three compounds exhibit good solubility in common organic solvents, such as CH_2Cl_2, THF, and DMSO. The thermal stabilities of these compounds have been investigated by thermogravimetric analysis (TGA), and the data is summarized in Figure S10. The decomposition temperatures (T_d) with a 5% weight loss are 337 °C for **Py-TPA**, 463 °C for **Py-2TPA,** and 436 °C for **Py-2TPE**, respectively. Moreover, the amount of carbonized residue

(char yield) of **Py-2TPE** is more than 55%, which is higher than for the compounds **Py-TPA** and **Py-2TPA**.

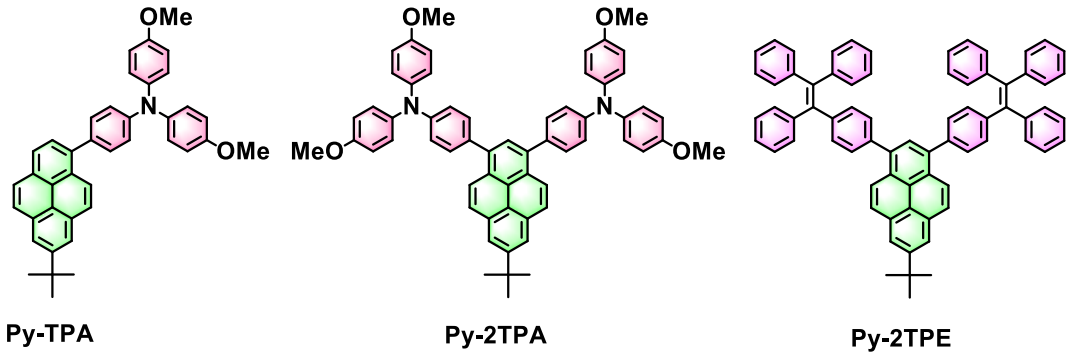

Figure 1. The designed pyrene-based molecules **Py-TPA**, **Py-2TPA,** and **Py-2TPE**.

3. Photophysical properties

The UV-vis absorption and emission spectra of the pyrene-based compounds **Py-TPA**, **Py-2TPA**, and **Py-2TPE** were measured in dilute THF solution (~10^{-5} M) and are presented in Figure S11. The key parameters are also summarized in Table 1. Due to the bulky groups at the 1,3-positions of pyrene, the compounds exhibit a broad and featureless absorption band in the range 240-450 nm, indicating that the substituents play an essential role in expanding the π-conjugation and lead to a charge transfer process.[25, 26] Compared to 2-*tert*-butylpyrene, the long-wavelength absorption peaks of **Py-TPA**, **Py-2TPA**, and **Py-2TPE** exhibit a significant hyperchromic shift to 371 nm, 362 nm, and 363 nm, respectively. As the number of substituents increased, the molar extinction coefficient (ε) was enhanced from 24790 (**Py-TPA**), 40447 (**Py-2TPA**) to 45009 M^{-1} cm^{-1} (**Py-2TPE**). On the other hand, due to the substituents at the 1,3-positions of pyrene, significant effects on the $S_1 \leftarrow S_0$ and $S_3 \leftarrow S_0$ transitions are experienced, but only slightly on the $S_2 \leftarrow S_0$ and $S_4 \leftarrow S_0$ transitions, and the shortest wavelength with the maximum absorption band is almost equal to that of the pyrenes.[27] In addition, the compounds **Py-TPA**, **Py-2TPA,** and **Py-2TPE** exhibited a similar absorption behavior with a slight red-shifted maximum absorption peak in six different polar solvents, which indicated that the electronic structure of the compounds in the ground state is independent of the solvent polarity (Figure S12).[28]

Both the TPA and TPE motifs are often exploited to construct AIEgens for potential applications in organic electronics,[29] bioimaging,[30] etc. To investigate the possible AIE feature of the compounds **Py-TPA**, **Py-2TPA** and **Py-2TPE**, their emission behavior was examined in dilute THF and THF/H_2O mixtures, as shown in Figure 2. The compound **Py-TPA** emits bright green emission with a maximum emission peak at 503 nm in THF solution. The

emission intensity gradually decreased with a red-shifted emission peak to 536 nm until the water fraction (f_w) was increased to 60%. On further increasing the f_w, the emission intensity was enhanced with a hyperchromic shift to 486 nm. A reasonable explanation for this fluorescence change is that the compound **Py-TPA** undergoes an intramolecular charge transfer (ICT) process, leading to a larger red-shifted emission when the $f_w \leq 60\%$, where the triphenylamine acts as a strong electron-donating group and the pyrene can act as an electron-withdrawing group. Furthermore, to remove the ICT effect, the PL spectra were performed in a mixture of dichloromethane and hexane (Figure S14). As the fraction of hexane increased, the emission intensity was enhanced with a blue-shifted emission peak from 520 to 438 nm. This is convincing evidence that the solvent polarity can lead to the large red-shifted emission of **Py-TPA** *via* the ICT process. On the other hand, due to the poor solubility of **Py-TPA** in water, it prefers to form aggregates at high f_w (> 60%), and the aggregated hydrophobic molecule excludes the solvent and leads to enhanced emission.[31] The quantum yield is 0.67 and 0.75 in the solution and solid state, respectively. Moreover, the fluorescence quantum lifetime (τ) of the compound **Py-TPA** was measured both in solution and in the thin film; details arsummarized in Table 1. The τ value was 1.2-fold enhanced in the thin film compared to that in solution. The calculated radiative decay rate (k_r) of **Py-TPA** is slightly decreased from 17.4 $\times 10^7$ s^{-1} to 16.6 $\times 10^7$ s^{-1} (*ca*. 0.95-fold), while the nonradiative decay rate (k_{nr}) is also decreased from 8.55×10^7 s^{-1} to 5.53×10^7 s^{-1} (*ca*. 0.65-fold). Moreover, the hyperchromic-shift emission may be attributed to the AIE effect overwhelming the ICT effect. Evidently, the **Py-TPA** exhibits a red-shifted emission of more than 150 nm, from blue (440 nm) to orange-red (560 nm), as the solvent polarity increased from cyclohexane (Cy) to dimethyl sulfoxide (DMSO) (Figure S12). The above results indicate that the compound **Py-TPA** is a bipolar molecule with a strong pull-push electronic structure, which displays an apparent solvatochromic effect. Thus, the **Py-TPA** is a blue aggregation enhanced emission (AEE) emitter with ICT characteristics.[31]

Table 1. Electrochemical and absorption and emission data of the pyrene-based compounds **Py-TPA**, **Py-2TPA**, and **Py-2TPE**

Compound	ε ($\lambda_{max\ abs}$) (M^{-1} cm^{-1})[a]	λ_{maxPL} (nm) solns[a]/ films[b]	Φ_f solns[a]/ films[b]	τ (ns) solns[a]/ films[b]	α_{AIE}[c]	k_r ($\times 10^7$ s^{-1})[d] solns[a]/ films[b]	k_{nr} ($\times 10^7$ s^{-1})[e] solns[a]/ films[b]
Py-TPA	371 / /24790	505/478	0.67/0.75	3.86/4.52	1.12	17.4/16.6	8.55/5.53
Py-2TPA	362 / 40447	509/490	0.62/0.07	4.39/8.93	0.11	14.1/0.8	8.66/10.4
Py-2TPE	363 / 45009	462/464	0.0046/0.47	0.89/1.79	102.17	0.52/26.3	112/29.6

[a] Maximum absorption wavelength measured in THF solution at room temperature. [b] Measured in the solid state, [c] $\alpha = \Phi_{solid}/\Phi_{soln.}$ [d] k_r = radiative decay rate (Φ/τ). [e] k_{nr} = nonradiative decay rate ($1/\tau$ - k_r).

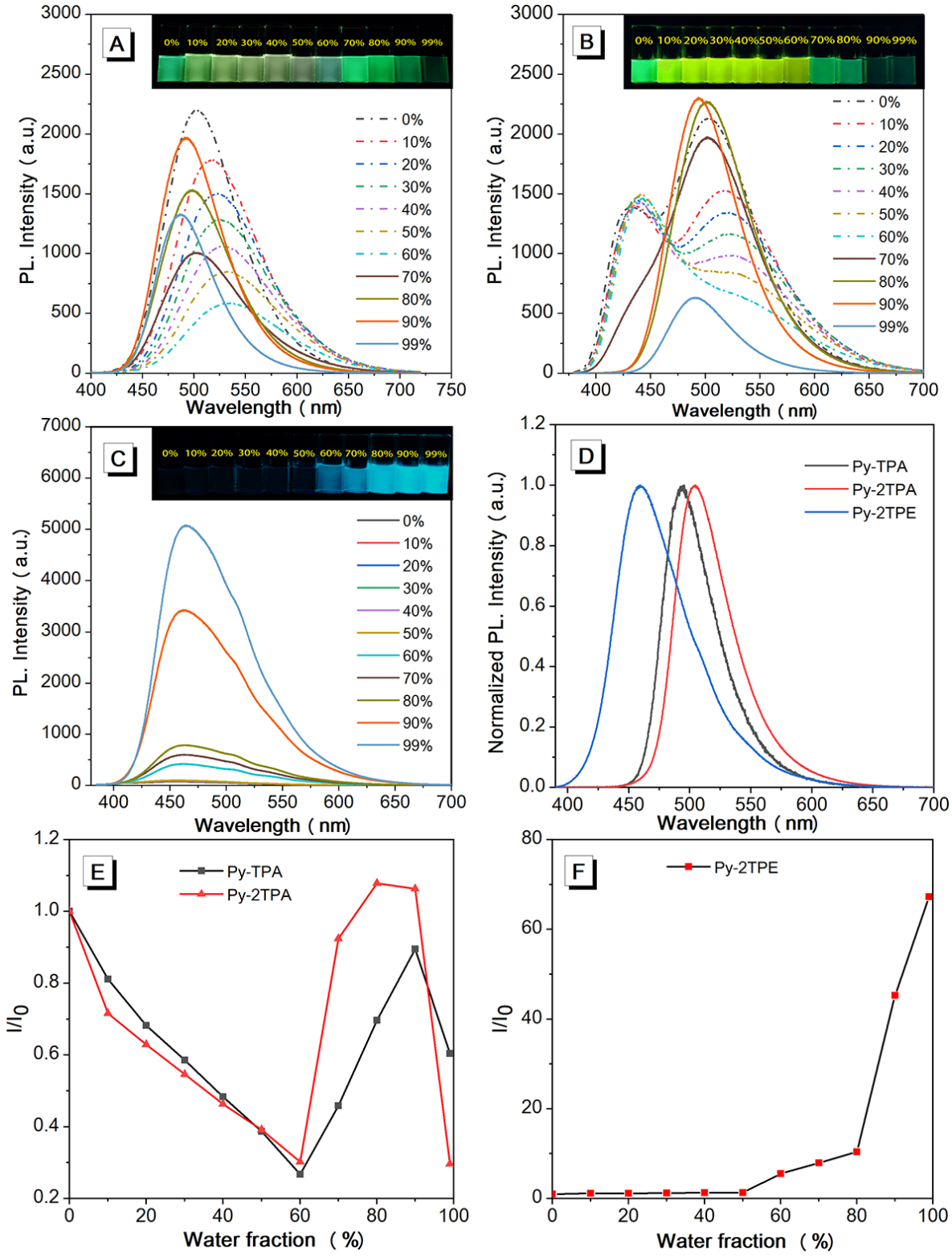

Figure 2. PL spectra of (A) **Py-TPA** (B) **Py-2TPA,** and (C) **Py-2TPE** in THF/water mixtures with different water fractions (f_w) (~10^{-5} M). (D) PL spectra of **Py-TPA**, **Py-2TPA,** and **Py-2TPE** in the solid-state. (E) and (F) The plot of relative PL intensity I/I_0. Inset: fluorescent

images of **Py-TPA**, **Py-2TPA,** and **Py-2TPE** in THF/water mixtures at different f_w taken under 365 nm UV irradiation.

Interestingly, the emission of compound **Py-2TPA** exhibits a dual emission with a maximum peak at 509 nm and a shoulder peak at 430 nm. As f_w increases to 60%, the long-wavelength emission intensity decreases with a red-shifted emission to 529 nm, which may be ascribed to the ICT effect. When f_w is in the range 70-90%, the emission peak at 430 nm also disappears with an enhancement of the emission peak at 510 nm (Figure 2B and E). Meanwhile the emission of compound **Py-2TPA** was almost quenched with a blue-shifted emission of 490 nm in the aggregated state (99%), meaning that the poorly soluble **Py-2TPA** prefers to form aggregates at high f_w, and the aggregated molecules exclude the solvent and limit the ICT effect, leading to a blue-shifted emission. In addition, as shown in Figure S14, the emission of the compound **Py-2TPA** was also measured in a mixture of dichloromethane and hexane. As the solvent polarity decreased, the long-wavelength emission peaks were blue-shifted from 520 to 436 nm, suggesting that the ICT effect is almost suppressed in the DCM/hexane (f_H = 99%) mixture with a large blue-shifted emission peak. The quantum yield of **Py-2TPA** decreased from 0.62 in solution to 0.07 in the thin film, indicating that it is an ACQ fluorophore. As shown in Figures 2C and F, the compound **Py-2TPE** is non-emissive in pure THF solution, and the emission intensity was enhanced *ca*. 70-fold as the water was gradually added from f_w = 0% to 99%. The quantum yield is enhanced to 0.47 in the solid-state *versus* THF solution (Table 1). The τ value of compound **Py-2TPE** was enhanced 2.0-fold in thin-film compared to in solution. The calculated k_r of **Py-2TPE** increased from 0.52 $\times 10^7$ s^{-1} to 26.3 $\times 10^7$ s^{-1}, while the nonradiative decay rate (k_{nr}) decreased from 112×10^7 s^{-1} to 29.6×10^7 s^{-1}. As expected, the **Py-2TPE** is a typical AIE-active molecule.

5. Fabrication of OLED devices.

Firstly, the blue emitters **Py-TPA** and **Py-2TPE** with high thermal stability were selected to fabricate doped blue OLEDs devices (D1-D8) with a configuration of ITO/HATCN (5 nm)/TAPC (50 nm)/TCTA (5 nm)/EML (20 nm)/ETL (30 nm)/LiF (1 nm)/Al, where 1,4,5,8,9,11-hexaazatriphenylene-hexacarbonitrile (HATCN), di-(4-(*N*,*N*-ditolyl-amino)-phenyl) cyclohexane (TAPC) and tris(4-carbazoyl-9-ylphenyl)amine (TCTA) were used as the hole injection layer, the hole transporting layer and the exciton blocking layer, respectively. The 2,2',2"-(1,3,5-benzinetriyl)-tris(1-phenyl-1-H-benzimidazole) (TPBi) and 1,3,5-tris(3-pyridyl-3-phenyl)benzene (TmPyPB) were used as the electronic transport layer (ETL) in the

construction of devices 1-4, respectively, and 4,4'-bis(*N*-carbazolyl)-1,1'-biphenyl (CBP) doped with 10 wt% of **Py-TPA** or **Py-2TPE** was used as the light-emitting layers.

Table 2. EL performance of blue OLEDs based on **Py-TPA** and **Py-2TPE**

Device	λ_{EL} (nm)	V (V)[b]	L (cd m^{-2})[a]	η_C (cd A^{-1})[a]	η_P (lm W^{-1})[a]	η_{ext} (%)[a]	η_r (%)	CIE (x, y)[c]
				maximum value / at 1000 cd m^{-2}				
D1	470	2.9	14280	6.86/5.77	7.18/3.61	4.67/3.94	31.3	(0.14,0.22)
D2	472	3.1	10337	8.38/6.70	8.23/4.57	5.28/4.21	35.2	(0.14,0.23)
D3	462	3.3	7217	5.63/4.96	4.77/3.31	3.84/3.40	40.9	(0.16,0.22)
D4	470	3.1	4881	11.99/7.92	11.78/5.41	7.12/4.71	75.7	(0.17,0.24)
D5	474	2.9	6348	9.65/5.10	10.11/3.34	5.77/3.05	38.5	(0.16,0.26)
D6	482	2.9	10290	12.28/6.51	12.86/4.55	6.11/3.24	40.7	(0.16,0.31)
D7	456	3.1	3928	9.62/5.89	9.45/3.65	6.12/3.75	65.1	(0.17,0.23)
D8	466	3.1	6651	12.65/8.02	12.42/5.48	7.27/4.60	77.3	(0.18,0.27)
D9	488	2.9	19712	15.16/14.58	13.72/11.76	6.53/6.29	43.5	(0.18,0.39)
D10	484	3.1	23162	11.23/11.23	9.67/8.06	4.90/4.90	52.1	(0.22,0.37)

Configuration:

Device 1 (**D1**): ITO/HATCN (5 nm)/TAPC (50 nm)/TCTA (5 nm)/10 wt% Py-TPA: CBP (20 nm)/TPBi (30 nm)/LiF (1 nm)/Al

Device 2 (**D2**): ITO/HATCN (5 nm)/TAPC (50 nm)/TCTA (5 nm)/10 wt% Py-TPA: CBP (20 nm)/TmPyPB (30 nm)/LiF (1 nm)/Al

Device 3 (**D3**): ITO/HATCN (5 nm)/TAPC (50 nm)/TCTA (5 nm)/10 wt% Py-2TPE: CBP (20 nm)/TPBi (30 nm)/LiF (1 nm)/Al

Device 4 (**D4**): ITO/HATCN (5 nm)/TAPC (50 nm)/TCTA (5 nm)/10 wt% Py-2TPE: CBP (20 nm)/TmPyPB (30 nm)/LiF (1 nm)/Al

Device 5 (**D5**): ITO/HATCN (5 nm)/TAPC (50 nm)/TCTA (5 nm)/mCP (5 nm)/5 wt% Py-TPA: PPF (20 nm)/TmPyPB (30 nm)/LiF (1 nm)/Al

Device 6 (**D6**): ITO/HATCN (5 nm)/TAPC (50 nm)/TCTA (5 nm)/mCP (5 nm)/10 wt% Py-TPA: PPF (20 nm)/TmPyPB (30 nm)/LiF (1 nm)/Al

Device 7 (**D7**): ITO/HATCN (5 nm)/TAPC (50 nm)/TCTA (5 nm)/mCP (5 nm)/5 wt% Py-2TPE: PPF (20 nm)/TmPyPB (30 nm)/LiF (1 nm)/Al

Device 8 (**D8**): ITO/HATCN (5 nm)/TAPC (50 nm)/TCTA (5 nm)/mCP (5 nm)/10 wt% Py-2TPE: PPF (20 nm)/TmPyPB (30 nm)/LiF (1nm)/Al

Device 9 (**D9**): ITO/HATCN (5 nm)/TAPC (50 nm)/TCTA (5 nm)/mCP (5 nm)/Py-TPA (20 nm)/PPF (5 nm)TmPyPB (30 nm)/LiF (1nm)/Al

Device 10 (**D10**): ITO/HATCN (5 nm)/TAPC (50 nm)/TCTA (5 nm)/mCP (5 nm)/Py-2TPE (20 nm)//PPF (5 nm)/TmPyPB (30 nm)/LiF (1nm)/Al

[a] The luminescence (L), current efficiency (η_c), power efficiency (η_P), and external quantum efficiency (η_{ext}) of the devices: maximum values/ values at 1000 cd m^{-2}; [b] Turn-on voltage at 1 cd m^{-2}; [c] CIE coordinates at 1000 cd/m^2.

The electroluminescent (EL) performance of the doped OLED devices D1-D4 is shown in Figures 3A-C, and the key EL parameters are summarized in Table 2. D1-D4 emit stable blue light with maximum EL peaks at 470 nm, 472 nm, 462 nm and 470 nm with corresponding Commission International Eclairage (CIE) coordinates of (0.14, 0.22), (0.14, 0.23), (0.16, 0.22) and (0.17, 0.24), respectively. The luminescence-voltage–current density (L–V–J) curve in D1 using **Py-TPA** as the light-emitting layer exhibits excellent EL characteristics with a low turn-on voltage of 2.9 V, a maximum luminescence (L_{max}) of 14280 cd m^{-2}, a maximum current efficiency ($\eta_{C\,max}$) of 6.86 cd A^{-1}, a maximum power efficiency ($\eta_{p\,max}$) of 7.18 lm W^{-1}, and an external quantum efficiency (EQE) of 4.67%. When the ETL was changed to TmPyPB, the EL performance of D2 was enhanced with $\eta_{C\,max}$, $\eta_{p\,max}$, and maximum EQE of 8.38 cd A^{-1}, 8.23

lm $W^{-1,}$ and 5.28%, respectively, but the L_{max} slightly decreased to 10337 cd/m^2. Similarly, for **Py-2TPE**, D4 displays a better EL performance using TmPyPB as the ETL compared to TPBi in D3. The $\eta_{C\ max}$, $\eta_{p\ max,}$ and maximum EQE were improved by more than 2-fold, up to 11.99 cd A^{-1}, 11.78 lm $W^{-1,}$ and 7.12 % in D4 compared to in D3. Therefore, the presence of the electron transport material TmPyPB can contribute to improving the EL properties of the blue OLED devices in these *Y*-shaped pyrene systems.

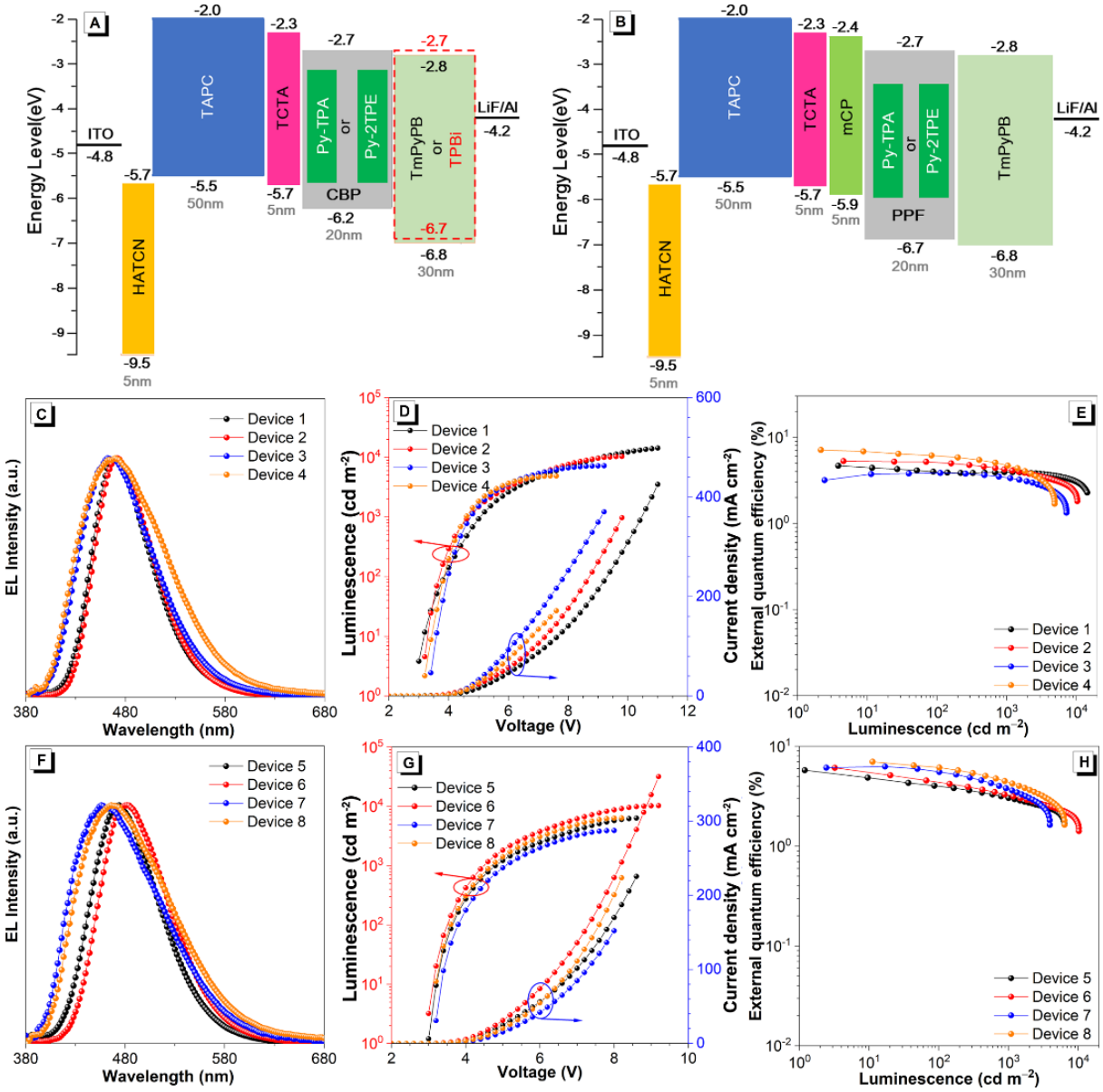

Figure 3. The schematic energy level diagram of related materials used in the fabrication of the OLED devices (A) for Devices 1-4, and (B) for Devices 5-8. (C) and (F) EL spectra recorded at 1000 cd m^{-2}. (D) and (G) luminance–voltage–current density (*L*–*V*–*J*) characteristics, (E) and (H) external quantum efficiency with the current density.

Thus, under the optimized conditions, we further investigated the effect of the doped host materials on the EL performance of the OLEDs. The emitting layer was replaced by 1,3-bis(carbazol-9-yl)benzene (mCP: served as the electron-blocking layer) doped with different concentrations (5 wt% or 10 wt%) of **Py-TPA** or **Py-2TPE**: PPF (2,8-bis(diphenylphosphoryl)dibenzo[b,d]furan, served as host material), corresponding to the devices D5, D6, D7, and D8. As the doping concentration increased, the maximum EL peaks of both devices D6 and D8 exhibited a slight red-shift (less than 10 nm) with better EL efficiencies compared to the devices D5 and D7. In particular, device D6 displayed the best performance with L_{max} of 10290 cd m^{-2}, $\eta_{c\ max}$ of 12.28 cd A^{-1}, $\eta_{p\ max}$ of 12.86 lm W^{-1}, and maximum EQE of 6.11% with CIE coordinates of (0.16, 0.31), while the L_{max}, $\eta_{ext\ max}$, $\eta_{c\ max}$, and $\eta_{p\ max}$ of the D8 are 6651 cd m^{-2}, 7.27%, 12.65 cd A^{-1}, and 12.42 lm W^{-1} with CIE of (0.18,0.27). Hence, the increased doped concentration of both emitters could improve the EL efficiency.

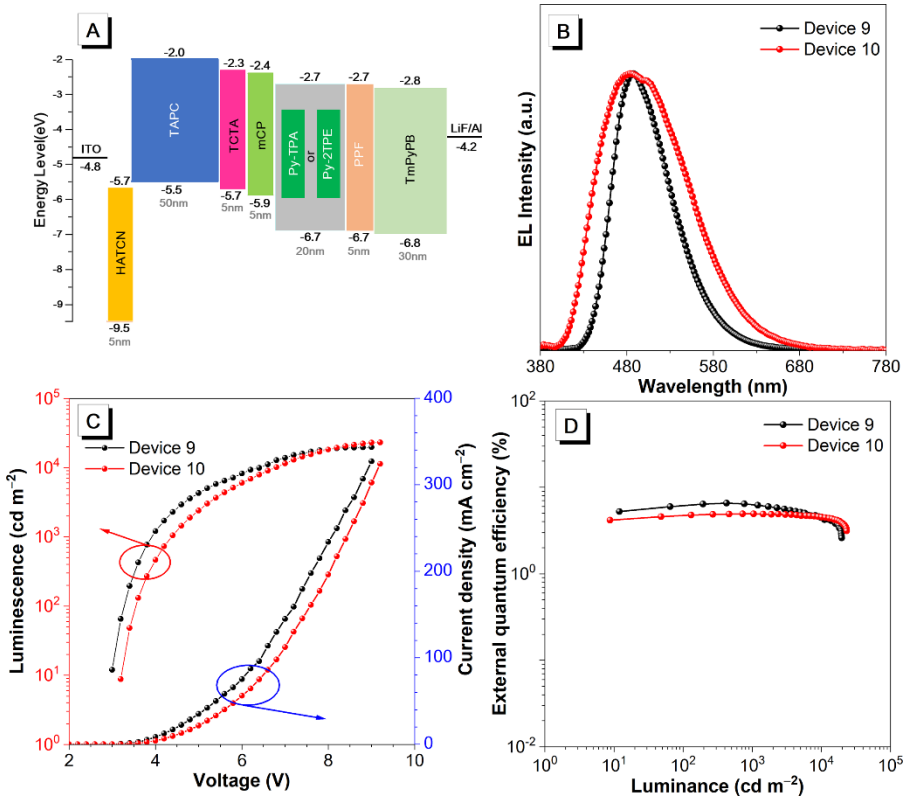

Figure 4. (A) The schematic energy level diagram of related materials used in the fabrication of the OLED Device 9 and Device 10; (B) EL spectra recorded at 1000 cd m^{-2}; (C) luminance–voltage–current density (L–V–J) characteristics; (D) external quantum efficiency with the current density.

For comparison, the non-doped OLED devices (D9-D10) were fabricated using the blue emitters **Py-TPA** and **Py-2TPE** as emitting layers, with a configuration of ITO/HATCN (5 nm)/TAPC (50 nm)/TCTA (5 nm)/mCP (5 nm)/emitter (20 nm)/PPF (5 nm)TmPyPB (30 nm)/LiF (1nm)/Al, respectively, where the functional layers of HATCN, TAPC, TCTA, and TmPyPB served as the hole injection layer, the hole transporting layer, the hole buffer and the electro-transport layers, respectively, while the mCP and PPF serve as exciton blocking layers. As shown in Figure 4, the non-doped OLED devices exhibit a red-shifted emission with a maximum EL peak at 488 nm for **Py-TPA** and 484 nm for **Py-2TPE**, compared to the doped OLEDs. However, the **Py-TPA** for the non-doped OLED (D9) exhibits a better EL characteristic compared to the doped-OLEDs (D1, D2, D5, and D6). In particular, the L_{max}, $\eta_{c\ max}$, $\eta_{p\ max}$, and maximum EQE are 19712 cd m^{-2}, 15.16 cd A^{-1}, 13.72 lm W^{-1}, and 6.63% with CIE coordinates of (0.18, 0.39), respectively. The non-doped OLED device (D10) of **Py-2TPE** shows a bright sky-blue emission with an EL peak at 484 nm with L_{max} of 23162 cd m^{-2}, with $\eta_{c\ max}$, $\eta_{p\ max}$, and maximum EQE of 11.23 cd A^{-1}, 9.67 lm W^{-1} and 4.90%. All devices D1-10 exhibit a low turn-on voltage, excellent EL characteristics, and low-efficiency roll-off. These results indicate that the pyrene-based AIEgens are great potential candidates for high-performance OLED applications, and strongly support our previous report.[22]

Theoretically, the EQE for traditional fluorescent OLEDs is less than 5%, while the maximum EQE for devices D2, D4, D5-D8, and D9 are breaking through the efficiency limit, indicating that the triplet excitons were utilized in these OLED devices. Firstly, according to the EL results, the good linear relationship between the current density and luminance curve of these devices (D1-D10) indicated that the potential triplet−triplet annihilation (TTA) should be excluded (Figure S16).[32] Subsequently, the η_r of each device was calculated according to the equation $\eta_{ext} = \gamma \times \eta_{PL} \times \eta_r \times \eta_{out}$, where γ is the electron-hole charge balance factor (ideally 100%), and η_{out} is the light extraction efficiency (≈ 20%). As shown in Table 2, the η_r for D1-D10 is 31.3% to 77.3%, and the **Py-2TPE**-based doped OLED device displays (D8) a maximum η_r of 77.3%. The high exciton utilization efficiency of these pyrene-based AIEgens is beneficial to achieving a high EQE, even higher than the theoretical value (5%).

6. Theoretical Calculations

The optimized molecular conformations and detailed electronic properties of the compounds **Py-TPA**, **Py-2TPA,** and **Py-2TPE** were investigated by the Gaussian 16 software. The ground state was calculated using the density functional theory (DFT) method at the B3LYP/6–31G (d,p) level, while the excited state was optimized using the time-dependent DFT method at the

M062X/6–31G (d,p) level. As shown in Figure 5A, three compounds exhibited twisted molecular geometries with torsion angles of 51.21-55.56° between the TPA (or TPE) unit and the pyrene core. In the ground state, the HOMO of compounds **Py-TPA** and **Py-2TPA** are spread over the TPA units and partially over the pyrene ring, and the LUMO is mainly distributed over the whole pyrene ring. The separation of the HOMO and LUMO levels indicates the bipolar characteristics of the molecules **Py-TPA** and **Py-2TPA**, where the TPA unit acts as an electron-donating group and the pyrene unit acts as an electron-withdrawn group. For **Py-2TPE**, the HOMO is predominantly distributed on the pyrene ring, and the LUMO is localized on the pyrene ring and partially over the TPE unit.

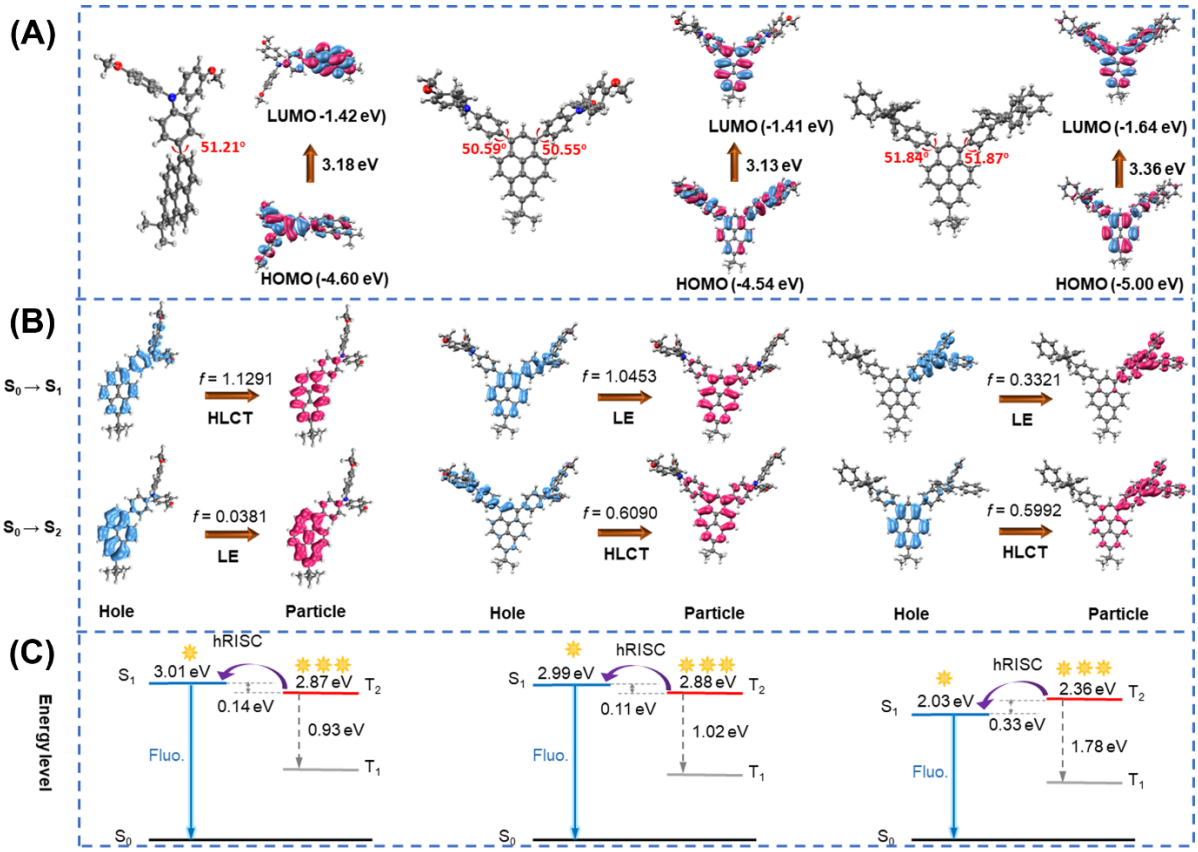

Figure 5. (A) The optimized ground-state conformations and the HOMO-LUMO distributions for **Py-TPA**, **Py-2TPA,** and **Py-2TPE** calculated at the B3LYP/6–31G(d, p) level; (B) Calculated NTO distributions for **Py-TPA**, **Py-2TPA,** and **Py-2TPE** of $S_0 \rightarrow S_1$ and $S_0 \rightarrow S_2$; (C) Schematic diagram of the energy-transfer process calculated at the M062X/6–31G(d, p) level.

The natural transition orbital (NTO) analysis was performed to understand the excited-state characteristics of **Py-TPA**, **Py-TPA,** and **Py-2TPE** (Figure 5B). For the $S_0 \rightarrow S_1$ transition of **Py-TPA**, the "hole" is distributed on the pyrene backbone and the fragment of triphenylamine, while the "particle" is mainly located on the pyrene backbone. For the $S_0 \rightarrow S_2$ transition, both

"hole" and "particle" are located on the pyrene core. The former can be assigned to a hybridized local and charge-transfer (HLCT) excited state, and the latter belong to the locally excited (LE) state with oscillator strength (*f*) values of 1.1291 and 0.0381, respectively. In contrast, the S_1 and S_2 of both **Py-2TPA** and **Py-2TPE** exhibit almost the same NTOs and are located on the pyrene ring and the TPA units, respectively. The $S_0 \rightarrow S_1$ transitions of both **Py-2TPA** and **Py-2TPE** display apparent LE state properties, and the $S_0 \rightarrow S_2$ transition displays HLCT state properties. Thus, the **Py-TPA** is an HLCT-dominated emitter, while **Py-2TPA** and **Py-2TPE** are LE-dominated emitters (Figure 5). On the other hand, for the $S_0 \rightarrow T_1$ transition, the "hole" and "particle" are mainly located on the pyrene ring for **Py-TPA**, **Py-2TPA**, and the TPE unit for **Py-2TPE**, respectively. For the $S_0 \rightarrow T_2$ transition, the "hole" and "particle" for the three compounds are mainly located on the pyrene ring (Figure S17). The vertical excitation energies (E_{VE}) were also examined based on the optimized singlet-state geometries. The compounds displayed a large energy gap between T_2 and T_1 of 0.93 eV for **Py-TPA**, 1.02 eV for **Py-2TPA**, and 1.78 eV for **Py-2TPE**, respectively. In contrast, as shown in Figure 5C, the energy gaps between S_1 and T_2 are small (0.14 eV for **Py-TPA**, 0.11 eV for **Py-2TPA**, and 0.33 eV for **Py-2TPE**). Thus, the unique electronic properties of these pyrene-based AIEgens play a significant role in harnessing the triplet excitons via a reverse intersystem crossing (RISC) process and improving the fluorescence and η_r value in the OLEDs.

7. Conclusion

In summary, three *Y*-shaped pyrene-based emitters were synthesized following the principle of aggregation-induced emission. The molecular structures and optical properties were fully characterized. The compounds **Py-TPA** and **Py-2TPE** exhibit a blue emission with AIE characteristics, while **Py-2TPA** is AIE inactive. Selected pyrene-based AIEgens were chosen for the fabrication of OLED devices. The L_{max} luminescence, η_{ext}, η_c, and η_p of the doped-OLED devices are 10290 cd m^{-2}, 6.11%, 12.28 cd A^{-1}, and 12.86 lm W^{-1} for **Py-TPA**, and 6651 cd m^{-2}, 7.27%, 12.65 cd A^{-1}, and 12.42 lm W^{-1} for **Py-2TPE** in the optimized OLED configurations, respectively. Moreover, the non-doped OLED devices for the pyrene-based AIEgens also display excellent EL properties with L_{max} of 23162 cd m^{-2}. In addition, all devices exhibited a low turn-on voltage in the range of 2.9-3.1 V. Theoretical calculations and NTO analysis revealed that the compounds **Py-TPA** and **Py-2TPE** can improve the η_r value in the OLEDs by a RISC process from the higher triplet T_2 to S_1. Thus, the pyrene-based AIEgens possess inherent advantages not only because of their blue emission properties and high quantum yields in the solid state but also due to the high η_r value and low turn-on voltage for

the OLED devices. This study provides an example of constructing pyrene-based AIEgens with high exciton utilization efficiency to fabricate the next-generation and highly efficient blue OLEDs.

8. Experimental Section

8.1. Materials

Unless otherwise stated, all reagents were purchased from commercial sources and were used without further purification. Tetrahydrofuran was distilled before use.

8.2. Characterization

^{1}H and ^{13}C NMR spectra were recorded on a Bruker AV 400M spectrometer using chloroform-*d*$_3$ or DMSO-d$_6$ solvent and tetramethylsilane as an internal reference. *J*-values are given in Hz. High-resolution mass spectra (HRMS) were recorded on a LC/MS/MS, which consisted of a HPLC system (Ultimate 3000 RSLC, Thermo Scientific, USA) and a Q Exactive Orbitrap mass spectrometer. UV-vis absorption spectra and photoluminescence (PL) spectra were recorded on a Shimadzu UV-2600 and the Hitachi F-4700 spectrofluorometer. PL quantum yields were measured using absolute methods using a Hamamatsu C11347-11 Quantaurus-QY Analyzer. The lifetime was recorded on an Edinburgh FLS 980 instrument and measured using a time-correlated single-photon counting method. Thermogravimetric analysis was carried on a Mettler Toledo TGA/DSC3+ under dry nitrogen at a heating rate of 10 °C/min. The quantum chemistry calculations were performed on the Gaussian 16 software package with B3LYP/6–31G(d, p) level for the ground state and M062X/6–31G(d, p) level for the excited state.

8.3. Synthesis of 4-(7-(*tert*-butyl)pyren-1-yl)-*N*,*N*-bis(4-methoxyphenyl)aniline (Py-TPA)

1-Bromo-7-(*tert*-butyl)pyrene (230 mg, 0.68 mmol, 1.0 eq.), 4,4'-dimethoxy-4'''-boronic acid triphenylamine (323 mg, 0.75 mmol, 1.1 eq.) and K_2CO_3 (400 mg, 2.8 mol, 2.8 eq.) were dissolved in a mixture of toluene/water/ethanol (10 mL, 2 mL, 2 mL) solvent in a round bottom flask under a nitrogen atmosphere. Tetrakis-(tri-phenylphosphine) palladium (100 mg, 0.086 mmol) was added, and the mixture was heated to 90 °C for 24 h. After cooling, it was extracted with dichloromethane, dried over magnesium sulfate, rotary evaporated, and finally separated by a chromatographic column to obtain a yellow product 4-(7-(*tert*-butyl)pyren-1-yl)-*N*,*N*-bis(4-methoxyphenyl)aniline (**Py-TPA**) (250 mg, yield 65%). ^{1}H NMR (400 MHz, DMSO-*d*$_6$, δ): 8.35 (d, *J* = 1.7 Hz, 1H), 8.32 (d, *J* = 1.7 Hz, 1H), 8.28 (d, *J* = 7.9 Hz, 1H), 8.18 (d, *J* = 9.4 Hz, 2H), 8.15 (d, *J* = 9.2 Hz, 2H), 7.95 (d, *J* = 7.9 Hz, 1H), 7.45 (d, *J* = 8.6 Hz, 2H), 7.20 – 7.14 (m, 4H), 6.98 (d, *J* = 8.0 Hz, 4H), 6.96 (d, *J* = 8.0 Hz, 2H), 3.77 (s, 6H), 1.55 (s, 9H) ppm; ^{13}C NMR (100 MHz, $CDCl_3$, δ): 149.4, 131.8, 131.3, 130.5, 127.8, 127.7, 125.8, 125.4, 124.9, 123.7,

122.7, 122.4, 115.0, 55.9, 35.6, 32.4 ppm; HRMS (ESI) *m*/*z*: $[M + H]^+$ calcd for $C_{40}H_{35}O_2$, 562.2741; found, 562.2740.

8.4. Synthesis of 4,4'-(7-(*tert*-butyl)pyrene-1,3-diyl)bis(*N*,*N*-bis(4-methoxyphenyl)aniline) (Py-2TPA)

1,3-Dibromo-7-(*tert*-butyl)pyrene (208 mg, 0.5 mmol, 1.0 eq), 4,4'-dimethoxy-4'-triphenylamine borate (436 mg, 1.25 mmol, 2.5 eq) and K_2CO_3 (500 mg, 3.6 mol, 3.6 eq.) were added to a 100 mL double neck flask, and then the solvents toluene (10 mL), ethanol (2 mL) and water (2 mL) were added. After stirring for 10 min., tetrakis(triphenylphosphine)palladium (120 mg, 0.1 mmol) was added, and the mixture was reacted at 90 °C for 24 h under a nitrogen atmosphere. Following this, it was extracted, filtered, and separated by chromatographic column to obtain the product 4,4'-(7-(*tert*-butyl)pyrene-1,3-diyl)bis(*N*,*N*-bis(4-methoxyphenyl)aniline) (**Py-2TPA**) (298 mg, yield 69%). According to the ^{1}H NMR spectra, small amounts of triphenylamine derivatives can not be removed by chromatographic column or vacuum sublimation. ^{1}H NMR (400 MHz, DMSO- d_6, δ): 8.31 (s, 1H), 8.19 (d, J = 9.3 Hz, 2H), 8.14 (d, J = 9.3 Hz, 2H), 7.83 (s, 1H), 7.48 (d, J = 8.6 Hz, 4H), 7.15 (d, J = 8.9 Hz, 8H), 6.94-6.98 (m, 12H), 3.76 (s, 12H), 1.55 (s, 9H) ppm; ^{13}C NMR (100 MHz, $CDCl_3$, δ): δ 156.0, 149.1, 141.0, 137.2, 131.4, 131.3, 127.5, 127.2, 126.8, 125.7, 125.5, 123.7, 122.0, 120.3, 114.8, 55.6, 32.0 ppm; HRMS (ESI) *m*/*z*: $[M + H]^+$ calcd for $C_{60}H_{52}N_2O_4$, 865.4011; found, 865.3995.

8.5. Synthesis of 7-(*tert*-butyl)-1,3-bis(4-(1,2,2-triphenylvinyl)phenyl)pyrene (Py-2TPE)

1,3-Dibromo-7-(*tert*-butyl)pyrene (208 mg, 0.5 mmol, 1.0 eq.), 1-(4-phenylboronic acid pinacol ester)-1,2,2-tristyrene (504 mg , 1.1 mmol, 2.2 eq) and K_2CO_3 (500 mg, 3.6 mol, 3.6 eq.) were added to a flask with the mixture solvent toluene (10 mL), ethanol (2 mL) and water (2 mL), and the system was stirred for 10 minutes, and then tetrakis(triphenylphosphine)palladium (120 mg, 0.1 mmol) was added. Following reaction at 90 °C for 24 h under a nitrogen atmosphere, on cooling, the mixture was extracted, filtered, and separated by a chromatographic column to afford the product 7-(*tert*-butyl)-1,3-bis(4-(1,2,2-triphenylvinyl)phenyl)pyrene **(Py-2TPE)** (261 mg, yield 56.8 %).^{1}H NMR (400 MHz, $CDCl_3$, δ): 8.21 (s, 2H), 8.10 (d, J = 9.2 Hz, 2H), 8.01 (d, J = 9.3 Hz, 2H), 7.89 (s, 1H), 7.41 (d, J = 8.0 Hz, 4H), 7.26 – 7.06 (m, 34H), 1.61 (s, 9H) ppm; ^{13}C NMR (100 MHz, $CDCl_3$, δ): 149.3, 144.0, 143.9, 143.9, 142.9, 141.5, 140.9, 139.2, 137.0, 131.6, 131.5, 131.4, 131.3, 130.1, 128.8, 127.9, 127.8, 127.8, 127.6, 126.7, 126.7, 126.6, 125.5, 125.3, 123.5, 122.3, 35.3, 32.1 ppm; HRMS (ESI) *m*/*z*: $[M + H]^+$ calcd for $C_{72}H_{54}$, 919.4298; found, 919.4305.

Supporting Information

Supporting Information is available from the Wiley Online Library or from the author.

Acknowledgements

J. Zeng, N. Qiu., and J. Zhang contributed equally to this work. This work was supported by the National Natural Science Foundation of China (21975054), Natural Science Foundation of Guangdong Province of China (2019A1515010925), Shenzhen Key Laboratory of Functional Aggregate Materials (ZDSYS20211021111400001), Guangdong Provincial Key Laboratory of Information Photonics Technology (2020B121201011), "One Hundred Talents Program" of the Guangdong University of Technology (GDUT) (1108-220413205), the Open Fund of Guangdong Provincial Key Laboratory of Luminescence from Molecular Aggregates, Guangzhou 510640, China (South China University of Technology) (2019B030301003), Science and Technology Planning Project of Hunan Province (2018TP1017), CR thanks the University of Hull for support. Thanks Dr. Zhiyang Liu from Southeast University for helpful discussions.

References

[1] C. W. Tang, S. A. VanSlyke, *Appl. Phys. Lett.* **1987**, 51, 913.
[2] X. Guo, P. Yuan, J. Fan, X. Qiao, D. Yang, Y. Dai, Q. Sun, A. Qin, B. Z. Tang, D. Ma, *Adv. Mater.* **2021**, 33, e2006953.
[3] D. Liu, M. Zhang, W. Tian, W. Jiang, Y. Sun, Z. Zhao, B. Z. Tang, *Aggregate.* **2022**, e164.
[4] C. Y. Chan, L. S. Cui, J. U. Kim, H. Nakanotani, C. Adachi, *Adv. Funct. Mater.* **2018**, 28, 1706023.
[5] X. Ai, E. W. Evans, S. Dong, A. J. Gillett, H. Guo, Y. Chen, T. J. H. Hele, R. H. Friend, F. Li, *Nature.* **2018**, 563, 536.
[6] M. A. Baldo, M. E. Thompson, S. R. Forrest, *Nature.* **2000**, 403, 750.
[7] L. Frederic, A. Desmarchelier, L. Favereau, G. Pieters, *Adv. Funct. Mater.* **2021**, 31, 2010281.
[8] M. Hasan, A. Shukla, V. Ahmad, J. Sobus, F. Bencheikh, S. K. M. McGregor, M. Mamada, C. Adachi, S. C. Lo, E. B. Namdas, *Adv. Funct. Mater.* **2020**, 30, 2000580.
[9] C. Murawski, K. Leo, M. C. Gather, *Adv. Mater.* **2013**, 25, 6801.
[10] W. Li, Y. Pan, R. Xiao, Q. Peng, S. Zhang, D. Ma, F. Li, F. Shen, Y. Wang, B. Yang, Y. Ma, *Adv. Funct. Mater.* **2014**, 24, 1609.
[11] D. Hu, L. Yao, B. Yang, Y. Ma, *Philos. Trans. R. Soc. A-Math. Phys. Eng. Sci.* **2015**, 373.
[12] H. Zhang, B. Zhang, Y. W. Zhang, Z. Xu, H. Z. Wu, P. A. Yin, Z. M. Wang, Z. J. Zhao, D. G. Ma, B. Z. Tang, *Adv. Funct. Mater.* **2020**, 30, 2002323.
[13] T. M. Figueira-Duarte, K. Mullen, *Chem. Rev.* **2011**, 111, 7260.
[14] M. M. Islam, Z. Hu, Q. Wang, C. Redshaw, X. Feng, *Mater. Chem. Front.* **2019**, 3, 762.
[15] L. Li, J. Y. Zhang, C. Y. Yang, L. Huang, J. Zhang, J. Bai, C. Redshaw, X. Feng, C. Y. Cao, N. J. Huo, J. B. Li, B. Z. Tang, *Small.* **2021**, 17, 2103125.

[16] X. Feng, J. Y. Hu, C. Redshaw, T. Yamato, *Chem. Eur. J.* **2016**, 22, 11898.
[17] X. Feng, Y. Du, X. Wei, T. Yamato, Pyrene-Based Advanced Luminescence Materials-Synthesis, Structure and Application, *China Science and Technology Press*, **2016**.
[18] J. Luo, Z. Xie, J. W. Lam, L. Cheng, H. Chen, C. Qiu, H. S. Kwok, X. Zhan, Y. Liu, D. Zhu, B. Z. Tang, *Chem. Commun.* **2001**, 1740.
[19] J. Mei, N. L. Leung, R. T. Kwok, J. W. Lam, B. Z. Tang, *Chem. Rev.* **2015**, 115, 11718.
[20] R. Hu, G. Q. Zhang, A. J. Qin, B. Z. Tang, *Pure Appl. Chem.* **2021**, 93, 1383.
[21] J. Yang, L. Li, Y. Yu, Z. Ren, Q. Peng, S. Ye, Q. Li, Z. Li, *Mater. Chem. Front.* **2017**, 1, 91.
[22] X. Feng, Z. Xu, Z. Hu, C. X. Qi, D. X. Luo, X. Y. Zhao, Z. F. Mu, C. Redshaw, J. W. Y. Lam, D. G. Ma, B. Z. Tang, *J. Mater. Chem. C.* **2019**, 7, 2283.
[23] Y. Liu, X. Man, Q. Bai, H. Liu, P. Liu, Y. Fu, D. Hu, P. Lu, Y. Ma, *CCS Chem.* **2022**, 4, 214.
[24] X. Feng, J. Y. Hu, C. Redshaw, T. J. C.-A. E. J. Yamato, *Chem. Eng. J.* **2017**, 22, 11898.
[25] X. Feng, J. Y. Hu, F. Iwanaga, N. Seto, C. Redshaw, M. R. Elsegood, T. Yamato, *Org. Lett.* **2013**, 15, 1318.
[26] T. M. Figueira-Duarte, S. C. Simon, M. Wagner, S. I. Druzhinin, K. A. Zachariasse, K. Mullen, *Angew. Chem. Int. Ed. Engl.* **2008**, 47, 10175.
[27] A. G. Crawford, A. D. Dwyer, Z. Liu, A. Steffen, A. Beeby, L. O. Palsson, D. J. Tozer, T. B. Marder, *J. Am. Chem. Soc.* **2011**, 133, 13349.
[28] H. B. Wang, J. N. Huo, H. B. Tong, X. H. Wei, Y. Zhang, Y. B. Li, S. M. Chen, H. P. Shi, B. Z. Tang, *J. Mater. Chem. C.* **2020**, 8, 14208.
[29] S. Ma, S. Du, G. Pan, S. Dai, B. Xu, W. Tian, *Aggregate.* **2021**, 2, e118.
[30] L. Xu, X. Jiang, K. Liang, M. Gao, B. Kong, *Aggregate.* **2021**, 3, e121.
[31] X. Y. Mao, F. L. Xie, X. H. Wang, Q. S. Wang, Z. P. Qiu, M. R. J. Elsegood, J. Bai, X. Feng, C. Redshaw, Y. P. Huo, J. Y. Hu, Q. Chen, *Chin. J. Chem.* **2021**, 39, 2154.
[32] V. Jankus, C. J. Chiang, F. Dias, A. P. Monkman, *Adv. Mater.* **2013**, 25, 1455.

_Y_-shaped pyrene-based aggregation-induced emission blue emitter for high-performance OLED Devices